Membrane Interactions of Cell-Penetrating Peptides Probed by Tryptophan Fluorescence and Dichroism Techniques: Correlations of Structure to Cellular Uptake†

Christina E. B. Caesar,‡ Elin K. Esbjörner,‡ Per Lincoln, and Bengt Nordén*

Department of Chemistry and Bioscience, Chalmers University of Technology, SE-41296 Gothenburg, Sweden

Received October 14, 2005; Revised Manuscript Received April 11, 2006

ABSTRACT: This work reports on the binding and conformation of a series of CPPs in the bilayer membranes of large unilamellar vesicles and the effect of the presence of cholesterol. We show a negative correlation between α-helical structure and uptake efficiency for penetratin peptides where the two central arginine residues of penetratin are thought to be important for breaking the secondary structure. Penetratin α-helicity is also reduced upon incorporation of cholesterol into the membrane. Flow linear dichroism in the far-UV region shows that the penetratin peptides adopt a preferential orientation of the α-helix parallel to the bilayer, and the linear dichroism (LD) spectrum in the aromatic region indicates that the tryptophan residues are preferentially oriented parallel to the membrane. The Tat analogue TatP59W and the oligoarginine R_7W, which are more efficient CPPs than penetratin, bind to membranes as random coils and do not show any orientation in LD, again indicating that α-helicity reduces uptake efficiency. Further, we observe large variations in tryptophan quantum yields for the five CPPs in this study and discuss this in terms of the ability to cause lipid rearrangement. Binding isotherms show that cholesterol increases the affinity of the peptide for the membrane, but tryptophan fluorescence lifetimes are essentially unaltered by incorporation of as much as 40 mol % cholesterol into the membrane, suggesting the absence of specific peptide−cholesterol interactions. Fluorescence emission maxima are insensitive to cholesterol and indicate that the peptide is positioned in the headgroup region. The results on peptide−membrane interactions are discussed in terms of possible uptake mechanisms.

Intracellular delivery of large molecules such as oligonucleotides and polypeptides for therapeutic applications is hampered due to the obstacle of crossing the hydrophobic plasma membrane. Since the discovery in 1988 that the HIV-1 Tat protein could enter cells (*1*, *2*), cell-penetrating peptides (CPPs)[1] have attracted considerable attention as highly efficient delivery vectors of hydrophilic cargo molecules. Tat peptides together with penetratin, a 16-residue peptide corresponding to the third helix of the Antennapedia homeodomain in *Drosophila*, are currently among the most commonly investigated CPPs. Tat peptides may vary slightly in sequence, although Vivès et al. showed that amino acids 48−60 correspond to the most efficient CPP. Deletion of three residues at the C-terminus (PPQ) has an only modest effect on uptake (*3*), whereas truncation or alanine substitution of any of the charged residues within the basic region of the peptide markedly reduced the rate of uptake (*4*). The uptake efficiency of Tat was attributed to the guanidinium headgroup of the arginine side chain rather than to positive charge alone since oligomers of arginine exhibited superior internalization characteristics compared to those of corresponding lysine, histidine, or ornithine oligomers (*4*).

CPPs were originally thought to cross plasma membranes in a receptor-, energy-, and temperature-independent, nonendocytotic manner (*5*, *6*). Peptide accumulation in the nucleus was often observed (*7*). The concept of an unknown passive diffusion process for a cationic peptide across the plasma membrane called for thorough investigations, both in vivo and in lipid model systems, for explaining the molecular basis of such a mechanism (*8*−*11*). In 2002 and 2003, research on CPP cell uptake took a drastic turn since Lundberg et al. (*12*), followed by Richard et al. (*13*), reported that cell fixation, even when using mild conditions, led to artifacts, in both uptake and intracellular distribution of peptides. Subsequent reports have shown that uptake of many CPPs, especially conjugated to cargo molecules, largely follows endocytotic routes. However, CPPs are able to deliver functional cargo, and cell entry, endocytotic or not,

† The Swedish Cancer Research Foundation is thanked for financial support.

* To whom correspondence should be addressed. E-mail: norden@chembio.chalmers.se. Telephone: +46-31-7723041. Fax: +46-31-7723858.

‡ These authors contributed equally to this work.

[1] Abbreviations: (11,12)-BrPC, 1-palmitoyl-2-stearoyl-11,12-dibromo-*sn*-glycero-3-phosphocholine; (6,7)-BrPC, 1-palmitoyl-2-stearoyl-6,7-dibromo-*sn*-glycero-3-phosphocholine; (9,10)-BrPC, 1-palmitoyl-2-stearoyl-9,10-dibromo-*sn*-glycero-3-phosphocholine; CD, circular dichroism; CPP, cell-penetrating peptide; DA, distribution analysis; DFQP, depth-dependent fluorescence quenching profile; DOPC, 1,2-dioleoyl-*sn*-glycero-3-phosphatidylcholine; DOPG, 1,2-dioleoyl-*sn*-glycero-3-phosphatidylglycerol; EDTA, ethylenediaminetetraacetic acid; HEPES, *N*-(2-hydoxyethyl)piperazine-*N*′-2-ethanesulfonic acid; LD, linear dichroism; LUV, large unilamellar vesicle; PM, parallax method; POPC, 1-palmitoyl-2-oleoyl-*sn*-glycero-3-phosphatidylcholine; POPG, 1-palmitoyl-2-oleoyl-*sn*-glycero-3-phosphatidylglycerol; TCSPC, time-correlated single-photon counting; TOE, tryptophan octyl ester.

10.1021/bi052095t CCC: $33.50
Published on Web 05/25/2006

must involve membrane interactions. We have previously reported that cationic CPPs can cross a pure lipid bilayer in giant unilamellar vesicles (*11*, *14*, *15*) but not in large (100 nm) unilamellar vesicles (LUVs). Others have recently proposed that translocation of penetratin into LUVs may be possible in the presence of a bilayer potential (*16*). Oligoarginines have been shown to readily be transferred from water to octanol in the presence of hydrophobic counterions, such as laureate. It has been suggested that transfer into the hydrophobic phase occurs due to charge neutralization of the arginine side chain guanidinium headgroup (*17*). Moreover, an oligoarginine consisting of seven arginines and a C-terminal tryptophan (R_7W), a Tat(48−60) peptide with residue 59 substituted with a tryptophan (TatP59W), and an arginine-enriched penetratin analogue (PenArg) have all been shown to enter PC-12 cells under conditions that abolish endocytosis (*18*). Even though elucidation of the detailed molecular mechanisms behind these phenomena is conceptually very interesting, it is rather more likely that the difference in efficiency among CPPs will be found in the cell surface interactions that direct these peptide−cargo constructs to follow different endocytotic routes. Tat−cargo constructs have been reported to internalize via caveolae (*19*) but also through macropinocytosis (*20*). Octaarginine uptake may also involve macropinocytosis, whereas penetratin seems to use a different route of entry (*21*). Saalik et al. (*22*) suggest that penetratin−avidin constructs are internalized via clathrin-dependent endocytosis but that clathrin-independent pathways must exist as well. Interestingly, in all the cases mentioned above, uptake is severely hampered by depletion of the level of cholesterol. Additionally, macropinocytosis has been suggested to be mediated through cholesterol-rich lipid rafts (*20*), making it relevant to study interactions between cholesterol and CPPs that use this route of entry.

In this report, membrane interactions of a series of CPPs have been characterized by a combination of tryptophan fluorescence and dichroism techniques using the phospholipid bilayers of LUVs as model membranes. Linear dichroism (LD) and circular dichroism (CD) have been used to address questions regarding conformation and orientation, whereas steady state and time-resolved fluorescence have been used to obtain information about the degree of peptide insertion and motional restriction. The data obtained for each peptide have been compared to the rate of cell uptake of its corresponding carboxyfluorescein-labeled analogue as reported in ref *18* in an effort to determine correlations between binding and uptake properties. Our set of CPPs includes the penetratin peptide and its two analogues, PenLys and PenArg (*18*), where penetratin's lysine residues have been substituted for arginines and vice versa, TatP59W and R_7W (see Table 1). All peptides contain at least one tryptophan (Trp) residue, which provides intrinsic optical properties that are sensitive to environmental change. The penetratin peptide contains two natural Trp residues which have been identified as being crucial to maintaining structure (*23*). TatP59W and R_7W have been equipped with one Trp residue each. Peptide sequences and their uptake efficiencies are listed in Table 1.

The influence of cholesterol on membrane binding has been investigated for 20 and 40 mol % cholesterol incorporated into the LUVs at the expense of zwitterionic DOPC. Apart from being important for efficient import of CPPs via endocytosis, cholesterol is a crucial component of eukaryotic membranes and has profound modulating effects on membrane properties. Cholesterol levels in membranes of living cells can approach 50% (*24*); a concentration of 30 mol % leads to significantly reduced membrane permeability (*25*), and at >25 mol %, there is a modulation of headgroup spacing leading to augmented hydration of the headgroups (*26*, *27*) but also enhanced motional freedom. Cholesterol adopts an orientation perpendicular to the membrane surface with the hydrophilic 3β-hydroxy group close to the lipid carbonyls lending the hydrophobic and rigid tetracyclic ring structure to cover approximately carbons 2−10 of the acyl chains (*28*). Moreover, cholesterol is not completely miscible with phospholipids over a wide range of concentrations (4−40 mol %) which may promote lateral segregation into cholesterol-rich and cholesterol-poor regions (*29*). Consequently, the two cholesterol levels used in this work, 20 and 40 mol %, can be regarded as representing the low and high regimes, respectively, of biologically relevant concentrations. It is also worth noting that the presence of cholesterol in the membrane of liposomes contributes to the increased rigidity of the membrane and leads to greater orientation of flow-aligned liposomes in linear dichroism measurements (unpublished data).

Table 1: CPP Sequences and a Summary of Our Earlier Results for Uptake Efficiency in Live Unfixed Rat Adrenal Pheochromocytoma Cells (PC-12) and Chinese Hamster V79 (Padua) Cells (*18*)[a]

		uptake efficiency		
peptide	sequence	37 °C	4 °C	ATP-depleted
penetratin	RQIKIWFQNRRMKWKK	+	−	−
PenArg	RQIRIWFQNRRMRWRR	++	+	+
PenLys	KQIKIWFQNKKMKWKK	−	−	−
TatP59W	GRKKRRQRRRPWQ	++	+	−
R_7W	RRRRRRRW	++	++	++

[a] The uptake efficiency was reported at 37 °C (normal conditions) as well as at 4 °C and after ATP depletion using rotenone (shutting down endocytosis). Uptake is characterized as either cell entry (+), efficient cell entry (++), or no cell entry (−).

EXPERIMENTAL PROCEDURES

Materials. 1,2-dioleoyl-*sn*-glycero-3-phosphatidylcholine (DOPC), 1,2-dioleoyl-*sn*-glycero-3-phosphatidylglycerol (DOPG), 1,2-dipalmitoyl-*sn*-glycero-3-phosphatidylcholine (POPC), and 1,2-dipalmitoyl-*sn*-glycero-3-phosphatidylglycerol (POPG) were from Larodan. 1-palmitoyl-2-stearoyl-6,7-dibromo-*sn*-glycero-3-phosphocholine [(6,7)-BrPC], 1-palmitoyl-2-stearoyl-9,10-dibromo-*sn*-glycero-3-phosphocholine [(9,10)-BrPC], and 1-palmitoyl-2-stearoyl-11,12-dibromo-*sn*-glycero-3-phosphocholine [(11,12)-BrPC] were from Avanti Polar Lipids. Tryptophan octyl ester (TOE), cholesterol, and sucrose (purity) were from Sigma. Standard buffers were 10 mM phosphate (pH 7.0) for the POPG/POPC lipid system and 100 mM NaCl, 10 mM HEPES, and 1 mM EDTA (pH 7.4) for the DOPG/DOPC lipid system. The peptides were synthesized by standard F-moc solid-phase chemistry with acetylated amino termini and amidated carboxyl termini as described previously (*11*). The peptides were purified via HPLC, and the sequence identity was verified using mass spectrometry. Absorption spectroscopy was used for concentration determinations using an extinction coefficient of 5690 M^{-1} cm^{-1} for Trp at 280 nm.

Preparation of LUVs. A dry lipid film was prepared from a chloroform solution through evaporation. LUVs were prepared by hydrating the lipid film in buffer by vortexing. Thereafter, the vesicles were subjected to five freeze−thaw cycles (liquid N_2/37 °C) before being extruded 21 times through 100 nm polycarbonate filters using a hand-held extruder or a LiposoFast-Pneumatic extruder (Avestin). All LUV preparations contained 20 mol % negatively charged lipid (POPG or DOPG). Addition of cholesterol (20 or 40 mol %) was always at the expense of the zwitterionic lipid (POPC or DOPC) to keep the surface charge constant. The peptide:lipid ratio was 1:100 in all experiments.

Flow Linear Dichroism (LD) Spectroscopy. LD is defined as the difference in absorption of linearly polarized light oriented parallel and perpendicular to a macroscopic orientation axis. Liposomes can be oriented by the shear flow between the two walls of a Couette cell as described in refs *30* and *31*. The shear causes a slight deformation of the liposomes which adopt an ellipsoidal shape with the longest dimension preferentially oriented parallel with the flow direction. By identifying the orientation of transition moments from peptide bonds and the tryptophan side chains, we can estimate an average orientation of the peptide relative to the membrane. All measurements where carried out on a Jasco J-720 spectropolarimeter equipped with an Oxley prism (*32*). Samples were oriented in a Couette cell with a total path length of 1 mm using a shear flow of 3100 s^{-1}. Spectra were recorded between 200 and 400 nm at ambient temperature. Prior to measurement, the samples were incubated for 2 h at room temperature. The buffer for all LD experiments contained 50% (w/w) sucrose to reduce light scattering from the liposomes and to increase the viscous drag (*30*).

Circular Dichroism (CD). CD is defined as the difference in the absorbance of left and right circularly polarized light. All CD measurements were performed on a Jasco J-810 spectropolarimeter using a 0.1 cm cell at 25 °C. All spectra were recorded between 190 and 250 nm, using 1 nm wavelength increments with a 0.5 s response and a bandwidth of 1 nm. Spectra were corrected for background contributions by subtracting appropriate blanks. The sensitivity and scan speed were set to 1 mdeg and 50 nm/min, respectively. Twenty scans were accumulated and averaged by the computer. Samples for CD were removed from the LD samples after measurement. The α-helical content was estimated from the mean residue molar ellipticities at 222 nm using the formula $[\alpha] = [\theta]_R/[-39500(1 - k/n)]$, where $[\alpha]$ is the α-helical fraction, k is a wavelength-dependent constant equal to 2.57 at 222 nm, and n is the number of amino acids in the peptide (*33*).

Steady State Fluorescence. Emission experiments were performed on a SPEX Fluorolog-3 spectrofluorimeter (JY Horiba) using a 1 cm × 1 cm quartz cell thermostated at 25 °C. The cuvette walls were modified with 1% polyethylenimine to minimize peptide adsorption as described previously (*34*). The excitation monochromator was set at 280 nm, and spectra were recorded between 315 and 400 nm in 1 nm increments. Excitation slits were set to 1 or 2 nm, with care taken to avoid photobleaching and scattering effects due to the lipid vesicles. Emission slits were set to 4 nm. Peptide concentrations were 1 μM, and the peptide:lipid molar ratio was 1:100. All emission spectra were corrected for background contributions and dilution. None of the membrane components, including cholesterol, has any significant absorption at the excitation wavelength, and tryptophan is the only fluorescent species.

Binding Isotherms. Data for binding isotherms were obtained by recording tryptophan emission spectra while titrating a LUV suspension with small volumes of peptide, added from a stock solution. The amount of free and bound peptide in each titration point was determined by a least-squares projection of the measured spectra on reference spectra corresponding to free and completely bound peptide (*34*).

Fluorescence Quantum Yields. Fluorescence quantum yields of the free peptide in solution were estimated relative to that of Trp in water. Sample concentrations were adjusted to give an absorbance of approximately 0.03, to avoid inner filter effects. Relative quantum yields were determined by summing the emission intensities in each point of the emission spectra and dividing by the absorbance. These ratios were compared to that of Trp which was set to 0.13 (*35*). The intensity increase upon binding to vesicles containing 0, 20, and 40 mol % cholesterol was determined by recording an emission spectrum of the free peptide, adding lipid vesicles, and measuring a new emission spectrum on the same sample to prevent concentration differences due to peptide adsorption in pipet tips, etc. (*34*).

Depth-Dependent Quenching of Tryptophan Fluorescence by Brominated Lipids. Quenching by brominated lipids was used to determine the bilateral position of the Trp residues which in turn gives an indication of the degree of insertion of the peptide into the membrane. Either (6,7)-, (9,10)-, or (11,12)-BrPC at 30 mol % was incorporated into LUVs together with appropriate amounts of DOPC, DOPG, and cholesterol. BrPC concentrations were determined by Fourier transform infrared spectroscopy on the lipid carbonyl stretch vibrations as described previously (*14*). Emission spectra were recorded in the absence (F_0) and presence [$F(h)$] of quencher, and the total intensity was taken as the sum of all measured points in each spectrum. The efficiency of quenching at each depth was reported as $F_0/F(h)$. Insertion depths were computed from the parallax equation (*36*) using quenching data from the two most efficient quenchers, namely, (6,7)-BrPC and (9,10)-BrPC:

$$Z_{CF} = L_{C1} + \frac{-\ln(F_1/F_2)/\pi C - L_{21}^2}{2L_{21}} \qquad (1)$$

where Z_{CF} is the distance from the tryptophan to the bilayer center, L_{C1} is the distance from the bilayer center to the shallowest located quencher and was set to 11 Å (*37*), L_{12} is the distance between the shallow and deep quencher (set to 2.7 Å), F_1 and F_2 are the tryptophan fluorescence intensities in the presence of the shallowest quencher and deepest quencher, respectively, and C is the surface concentration of quencher and was determined by assuming that the average cross-sectional area of DOPC, DOPG, and BrPC lipids is 70 $Å^2$ (*38*) and that the corresponding area of cholesterol is 38 $Å^2$ (*39*).

Time-Resolved Fluorescence Spectroscopy. Fluorescence lifetimes were measured using time-correlated single-photon counting (TCSPC). The excitation source was the frequency-tripled output from a Ti:sapphire oscillator (Tsunami, Spectra

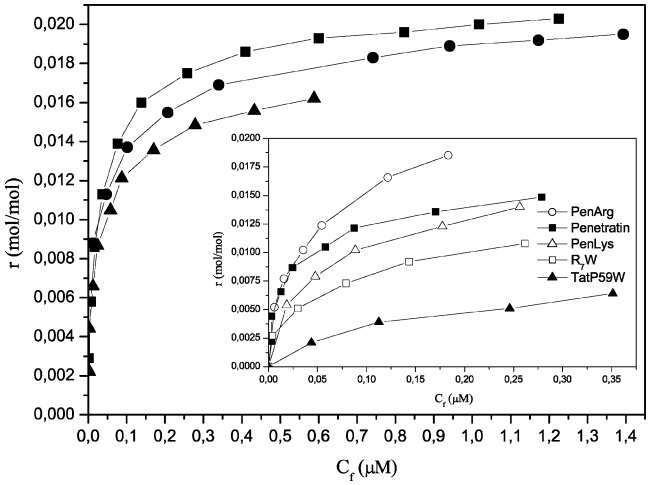

FIGURE 1: Binding isotherms for the association of penetratin with DOPC/DOPG vesicles containing 0 (▲), 20 (●), and 40 mol % cholesterol (■). The membrane-bound peptide:lipid molar ratio, *r*, is plotted vs the concentration of free peptide in bulk solution (C_f). In the inset are binding isotherms for PenArg, penetratin, PenLys, R_7W, and TatP59W in DOPC/DOPG vesicles containing no cholesterol.

Physics), pumped by a continuous-wave frequency-doubled diode pumped Nd:YVO4 laser (Millennia Pro, Spectra Physics). The excitation light was frequency modulated to 8 MHz by a model 3850 pulse picker (Spectra Physics). The photons were collected by a microchannel plate photomultiplier tube (MCP-PMT R3809U-50, Hamamatsu) and fed into a multichannel analyzer with 4096 channels yielding a maximum time resolution of 10 ps. The excitation wavelength was set to 280 nm, and emission was recorded using magic-angle conditions at 350 nm for peptides free in solution and 337 nm for peptides associated with liposomes. The band-pass of the monochromator was 8 nm. At least 10^4 counts were collected in the top channel. The intensity data were fitted by iteratively reconvoluting a triexponential expression with the instrument response signal using the software package F900 (Edinburgh Instruments). The instrument response signal was recorded using a diluted silica sol scattering solution for free peptide measurements. For the membrane-bound peptide, it was desirable to mimic the scattering in the sample, and therefore, a 100 μM liposome suspension was used as the scattering solution, whereafter peptide was added and the fluorescence decay measured.

RESULTS

Peptide Binding. Binding isotherms were constructed by projection of tryptophan emission spectra, recorded during titration of a LUV suspension with peptide from a stock solution, onto reference spectra of free and bound peptide. The bound peptide:lipid molar ratio, *r*, was plotted versus the free peptide concentration in bulk solution in Figure 1 which shows binding of penetratin to DOPC/DOPG LUVs containing 0, 20, and 40 mol % cholesterol. The figure shows that peptide binding becomes more efficient when cholesterol is incorporated. However, in the region of the binding isotherm where the experiments of this study were performed (at a peptide:lipid ratio of 1:100), the differences are marginal. The inset shows binding isotherms for all five peptides in DOPC/DOPG LUVs. There is a variation in binding efficiency among the different peptides, and this result is in good agreement with binding isotherms describing the binding of these peptides to membranes with 40 mol % negative charge (*15*, *23*). The penetratin peptides exhibit a high degree of binding (~95%) at a peptide:lipid ratio of 1:100 and a total peptide concentration of 1 μM, whereas R_7W and TatP59W have lower membrane affinities.

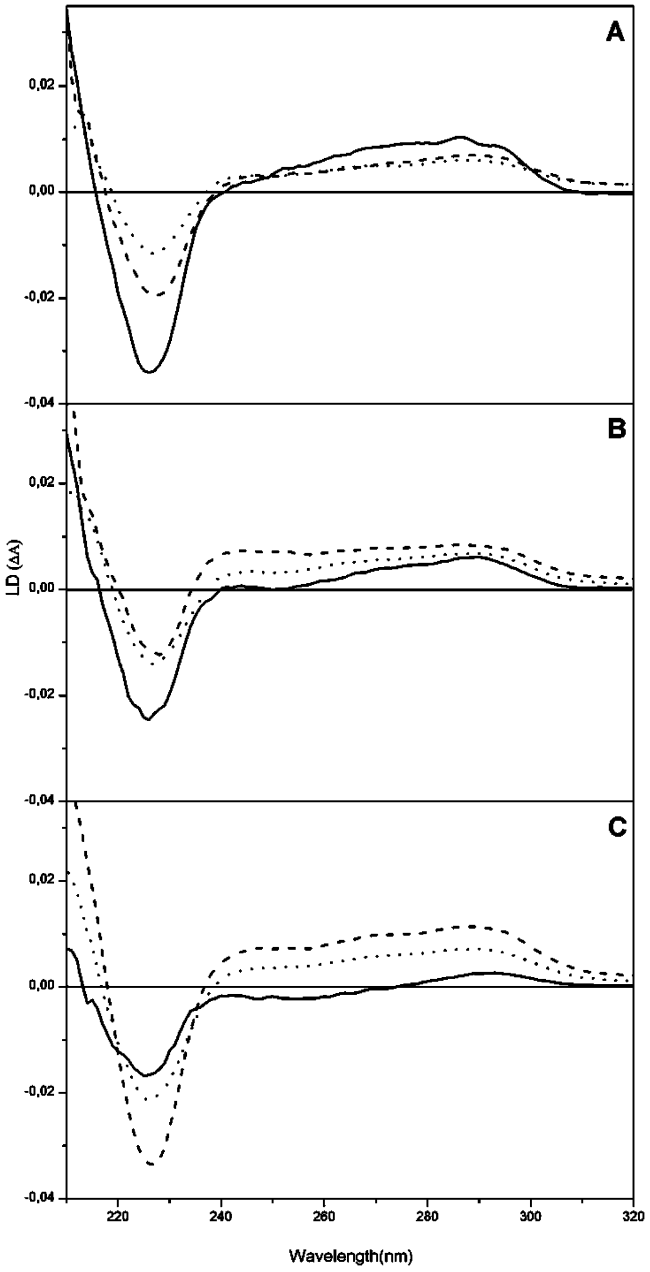

FIGURE 2: LD spectra of (A) penetratin, (B) PenArg, and (C) PenLys in POPC/POPG vesicles containing 0 (—), 20 (···), and 40 mol % cholesterol (- - -).

Linear Dichroism. LD spectra for penetratin, PenArg, and PenLys are presented in Figure 2. Since TatP59W and R_7W contain only random coil secondary structure, these peptides as expected do not exhibit any peptide-specific LD. In an α-helix, the $\pi \rightarrow \pi^*$ transitions of the amide chromophores interact by exciton coupling to give two transitions: one at a longer wavelength (200−210 nm) polarized parallel to the helix axis and one at a shorter wavelength (180−200 nm) perpendicular to the helix axis. In addition, an $n \rightarrow \pi^*$ transition at 210−230 nm is polarized perpendicular to the helix axis. Penetratin, PenArg, and PenLys all have in

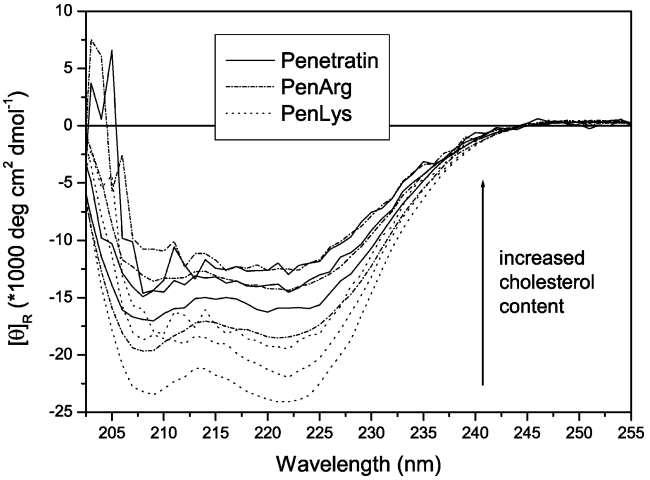

FIGURE 3: CD spectra of penetratin (—), PenArg (- - -), and PenLys (•••) in POPC/POPG vesicles containing 0, 20, or 40 mol % cholesterol. The arrow shows the direction of spectral change upon incorporation of cholesterol.

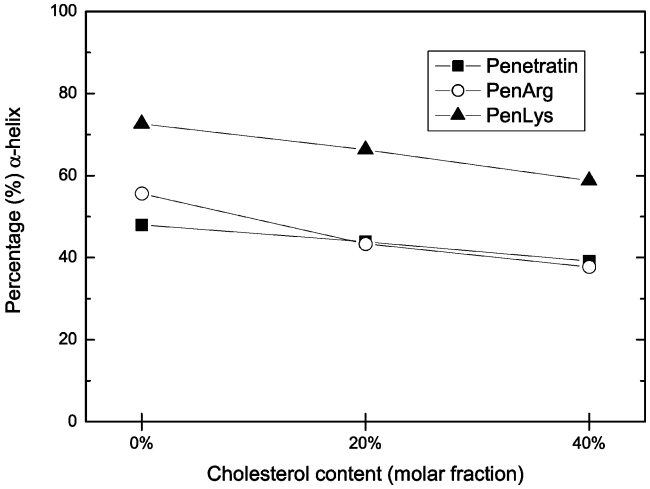

FIGURE 4: Estimated α-helical content (%) of penetratin (■), PenArg (○), and PenLys (▲) when bound to POPC/POPG vesicles containing 0, 20, or 40 mol % cholesterol.

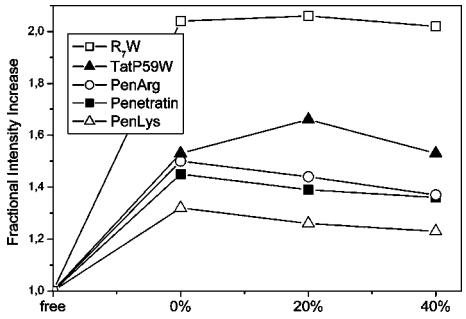

FIGURE 5: Fractional intensity increase of total Trp emission upon addition of LUVs containing 0, 20, and 40 mol % cholesterol to a 1 μM peptide solution. The emission intensities are normalized with respect to the emission of the free peptide. Binding experiments (Figure 1) have shown that as much as 30% of TatP59W may be free in solution at a total peptide:lipid molar ratio of 1:100 at the ambient peptide concentration. If this fraction of free peptide is taken into consideration, the actual increase in fluorescence quantum yield of the bound peptide should be higher than in the figure. Estimations for TatP59W in LUVs without cholesterol indicate that the increase in quantum yield for the fraction of bound peptide may be approximately 1.8.

common the fact that the α-helical part of the peptide is oriented with the helix axis parallel to the surface of the liposome membrane, as indicated by a negative LD at the n → π* transition at 226 nm and a positive LD at 208 nm (parallel $\pi \rightarrow \pi$* transition). The orientation of the α-helical part of the peptides is not changed when they bind to vesicles containing 20 or 40 mol % cholesterol; the overall sign of the LD is maintained, although the negative magnitude of the n → π* transition at 226 nm is affected by cholesterol content. Additional information about peptide orientation can be obtained from the 220−290 nm region where the indole chromophore of the tryptophan side chain absorbs. Indole has three transitions corresponding to the following absorption bands: the B_b band, the broad and unstructured L_a band, and the vibrationally structured L_b band. Both penetratin and PenArg exhibit positive LD in the L_a−L_b region for all vesicle types. This indicates an average orientation of the plane of the indole moieties parallel to the membrane surface. In the absence of cholesterol, PenLys has a positive LD for the L_b transition but a negative LD for the L_a transition. These data suggest that the Trp residues tilt into the membrane.

Circular Dichroism. CD spectra were recorded in the absence and presence of cholesterol for penetratin, PenArg, and PenLys (Figure 3) and for TatP59W and R_7W (data not shown). Free in solution, all peptides exhibit random coil secondary structure. Figure 3 clearly shows that the penetratin peptides adopt α-helical conformations when binding to vesicles, whereas TatP59W and R_7W have typical random coil spectra indicating that they remain unstructured (data not shown). Accurate signals could not be recorded below 200 nm due to the large amount of sucrose in the samples. The α-helical content of membrane-bound peptide as a function of vesicle cholesterol content is presented in Figure 4. The α-helical contents were estimated from the mean residue molar ellipticities at 222 nm as described in Experimental Procedures and are in good agreement with previous results with similar LUV membranes and in buffers without sucrose (*23*).

Fluorescence Quantum Yields. The fluorescence quantum yields were determined relative to that of free Trp (0.13). All peptides had quantum yields of ∼0.11 in buffer (data not shown), but the intensity increase upon binding to vesicles exhibited noticeable differences. The fractional increase in total Trp emission intensity upon addition of lipid vesicles to a 1 μM peptide solution are presented in Figure 5. The penetratin peptides all show a decrease in emission intensity when the lipid vesicle cholesterol content is increased, whereas R_7W has a rather similar intensity independent of cholesterol content. TatP59W shows a slight increase in intensity when it is bound to LUVs containing 20% cholesterol. The arginine-rich peptides in this study (PenArg, TatP59W, and R_7W) appear to have the greatest increase in emission intensity upon binding to vesicles, whereas PenLys, which entirely lacks arginines, shows the smallest intensity increase. Emission maximum wavelengths are blue-shifted approximately 12 nm for the penetratin peptides and somewhat less for TatP59W and oligoarginine. Incorporation of cholesterol into the LUVs has an apparently negligible effect on the emission maximum wavelengths which vary less than 1 nm in all cases (see Table 2).

Depth-Dependent Quenching of Tryptophan Fluorescence by Brominated Lipids. Depth-dependent quenching of tryptophan fluorescence was used to estimate the bilateral

Table 2: Tryptophan Emission Maximum Wavelengths (nanometers) of Peptides in Solution (free) and Bound to DOPC/DOPG Vesicles with 0, 20, and 40 mol % Cholesterol

	free	0 mol %	20 mol %	40 mol %
penetratin	349	338	337	337
PenArg	349	337	336	336
PenLys	349	337	336	336
TatP59W	350	342	340	341
R_7W	349	341	340	341

position of Trp and, hence, the approximate insertion of the peptides in lipid vesicles containing varying amounts of cholesterol. Table 3 shows the degree of quenching, F_0/F_Q, represented as the ratio of the total emission intensity in vesicles without quencher to the total emission intensity in vesicles containing quencher at a certain position along the acyl chain. Quenching is most efficient in vesicles with (6,7)-BrPC followed by (9,10)-BrPC, whereas the level of quenching is much lower in (11,12)-BrPC vesicles. The quenching ratios are the average values of two or three independent measurements. The maximum variation in any of the measurements was 3.3%, and the average variation was 0.8%. In general, the peptides exhibit a trend of an increased level of quenching with increased cholesterol content in vesicles containing (6,7)-BrPC and (9,10)-BrPC, with the effect being most pronounced when going from 20 to 40% cholesterol. The tryptophan insertion was estimated using the parallax equation as described in Experimental Procedures, and the distances from the bilayer center, Z_{CF}, are listed in bold in Table 3. The maximum emission wavelengths of the tryptophans in each peptide in the presence of different quenchers do not vary to any appreciable extent (data not shown). This suggests that all peptide molecules in a sample bind in a similar fashion and that the two tryptophan residues in the penetratin peptides have similar bilateral positions in the membrane.

Time-Resolved Fluorescence Spectroscopy. The fluorescence decay parameters of the Trp residue(s) in the peptides were determined, in the absence and presence of POPG/POPC lipid vesicles containing 0, 20, or 40 mol % cholesterol. The fluorescence curves could not be satisfactorily fitted using a sum of fewer than three exponential decays for both free and membrane-bound peptides, but also for the model compound TOE. The lifetimes, together with normalized preexponential factors, are plotted in Figure 7. χ^2 values were less than 1.3 in all measurements. The lifetimes for tryptophan in buffer have been determined to be 3.1 and 0.65 ns.

DISCUSSION

The binding of cationic peptides to a negatively charged membrane surface is dependent on both electrostatic and hydrophobic interactions. A binding model based on combining Gouy−Chapman theory with a surface partition equilibrium (*40*) has previously been used to successfully describe binding of the penetratin peptides as well as TatP59W and R_7W to model membranes containing 40 mol % negatively charged lipids (*15*, *23*). The effect of surface charge density on binding has also been thoroughly investigated for penetratin (*34*). From these studies, it is evident that the formation of both inter- and intramolecular bonds when the peptide forms an α-helix upon membrane association decreases the free energy of binding. This hydrophobic effect is virtually independent of the amount of negative charge as is the degree of α-helicity. By contrast, the electrostatic contribution to the binding energy is highly dependent on the surface charge density.

Figure 1 shows that the binding efficiency of penetratin is dependent on membrane cholesterol, with binding being increasingly stronger upon incorporation of 20 and 40 mol % cholesterol. Such a behavior has been previously observed for the amphipathic Ac-18A-NH_2 peptide which also is located in the interfacial region of the membrane (*41*). Cholesterol was incorporated into the lipid vesicles at the expense of zwitterionic DOPC, and due to a smaller cross-sectional area of cholesterol (∼37 Å^2) versus DOPC (65−70 Å^2) (*38*, *39*, *41*, *42*), there is an increase in surface charge density upon cholesterol incorporation. This could affect the electrostatic contribution to binding energy and explain the stronger binding. However, incorporation of cholesterol also leads to a decreased α-helical content, which in turn is likely to affect the hydrophobic contribution to the free energy of binding. Importantly, the effect of membrane cholesterol is minor in the peptide concentration region where our experiments have been performed (total peptide:lipid ratio of 1:100). The variations in binding affinity between different peptides are more pronounced, as seen in the inset of Figure 1. The penetratin peptides exhibit stronger binding than TatP59W and R_7W do which may reflect the importance of hydrophobicity in addition to electrostatic contributions at

Table 3: Degree of Tryptophan Quenching by Brominated Lipids and Estimated Insertion Depths, Z_{CF} (reported as the distance from the bilayer center)[a]

	0% cholesterol[b]				20% cholesterol[b]				40% cholesterol[b]			
	F_0/F_Q				F_0/F_Q				F_0/F_Q			
	(6,7)[c]	(9,10)[c]	(11,12)[c]	Z_{CF}[d] (Å)	(6,7)[c]	(9,10)[c]	(11,12)[c]	Z_{CF}[d] (Å)	(6,7)[c]	(9,10)[c]	(11,12)[c]	Z_{CF}[d] (Å)
penetratin	1.74	1.59	1.32	**10.9**	1.78	1.55	1.29	**11.4**	2.31	1.88	1.29	**12.0**
PenArg	1.80	1.68	1.34	**10.6**	2.02	1.74	1.32	**11.6**	2.47	2.03	1.36	**11.9**
PenLys	1.70	1.60	1.28	**10.5**	1.94	1.62	1.28	**11.9**	2.17	1.79	1.26	**11.8**
TatP59W	1.44	1.35	1.12	**10.5**	1.91	1.67	1.44	**11.4**	1.53	1.35	1.02	**11.1**
R_7W	1.75	1.58	1.20	**11.0**	2.02	1.71	1.33	**11.8**	2.10	1.69	1.13	**12.1**

[a] Tryptophan quenching is tabulated as the ratio of the fluorescence intensity in the absence of quencher (F_0) and in presence of quencher (F_Q) at a specified position on the hydrocarbon tail. The insertion depths have been computed using the parallax equation. The maximum variation in the quenching data was 3.3%, and the average variation was 0.8%. [b] Molar fraction of cholesterol in the LUVs. All LUVs contained 30 mol % brominated lipid and 20 mol % negatively charged DOPG. Addition of cholesterol was always at the expense of zwitterionic DOPC. [c] Quencher position along the lipid acyl chain. (6,7) corresponds to a position 11 Å from the bilayer center, (9,10) 8.3 Å, and (11,12) 6.5 Å. [d] Average distance from the bilayer center. The hydrocarbon core region stretches approximately 15 Å from the center in a DOPC membrane.

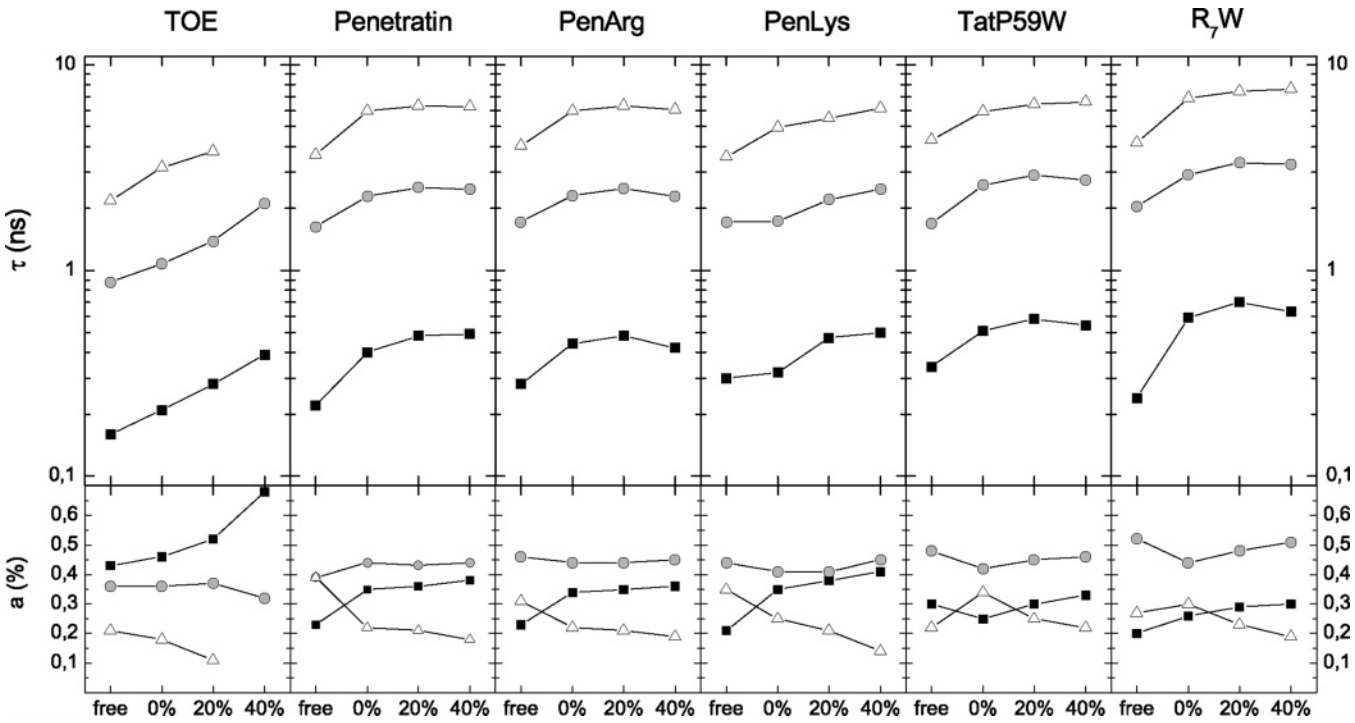

FIGURE 6: Tryptophan fluorescence lifetimes (τ) for peptide in buffer (free) and peptide bound to POPC/POPG vesicles containing varying amounts of cholesterol (0, 20, or 40 mol %) and the corresponding preexponential factors (α).

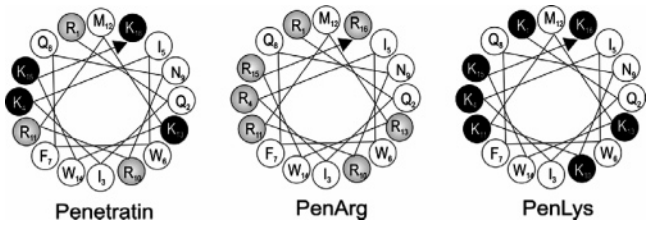

FIGURE 7: α-Helical wheel presentation of penetratin, PenArg, and PenLys. Arginine residues are highlighted in gray and lysine residues in black.

this surface charge ratio. R_7W binds significantly more strongly than TatP59W even though the latter peptide has one additional positive charge (+8 compared to +7 for R_7W). This finding may be attributed to the superior binding ability of arginines compared to that of lysines which is also evident from the order of binding strength for the penetratins (PenArg > Pen > PenLys). The degree of binding is an important parameter to consider when interpreting data from the fluorescence experiments which were performed using a total peptide concentration of 1 μM. The CD and LD data were recorded at a much higher total concentration (but at the same peptide:lipid molar ratio). As seen from the binding isotherms, at a fixed peptide:lipid molar ratio, the relative amount of bound peptide increases substantially when the total peptide concentration increases. For example, for TatP59W approximately 97% is bound at a peptide concentration of 25 μM and a peptide:lipid ratio of 1:100.

The CD experiments show that all three penetratin peptides have α-helical structure when bound to liposome membranes (Figures 3 and 4). Moreover, the secondary structure of membrane-bound penetratin peptides appears to be sensitive to the presence of membrane cholesterol since all peptides exhibit a decrease in α-helical content with an increase in the amount of cholesterol. TatP59W and R_7W remain unstructured in all vesicle types. The peptide bond region of the LD spectra indicates that the α-helical parts of the penetratin peptides are oriented parallel to the lipid bilayer surface. The overall orientation of the helix does not change when cholesterol is incorporated into the bilayer. Because of the partly amphipathic nature of the penetratin α-helix (see Figure 7 for a helical wheel representation), partitioning into the interfacial bilayer region is expected. Adopting an orientation parallel to the bilayer would minimize thermodynamically unfavorable contacts between hydrophobic amino acid residues and the membrane surroundings as well as optimize favorable contacts between polar residues and charged lipid headgroups. Evidence for strong interfacial interactions of both aromatic (Trp and Tyr) and positively charged (Lys and Arg) amino acids can be found in the literature (*43*).

LD cannot distinguish between the two Trp residues in the penetratin peptides if they are in very similar environments, and consequently, an average LD spectrum is obtained. Indeed, the similarity in spectral structure between the LD and absorption spectrum at 270−300 nm is thus a strong indication that both Trps are in the same environment. Also, the fact that the Trp emission maxima are insensitive to quenching by brominated lipids at different levels within the membrane indicates that both Trp residues reside at the same depth. If the two Trps in penetratin had resided at different depths, they would have exhibited different emission maxima and the obtained emission spectrum would have been an average spectrum. In LUVs containing brominated lipids, these Trps would be unequally quenched, and hence, there would be a shift in the emission maximum wavelength. The existence of one Trp distribution also justifies the use of the average LD signal to describe the Trp orientation and supports LD data showing a parallel orientation for the α-helical part of the peptides. Furthermore, this finding strengthens evidence from a previously published report about the membrane orientation of penetratin (*44*) suggesting

that the residues not taking part in the α-helix stretch out parallel to the membrane surface. In penetratin, the two Trp residues are located at positions 6 and 14 from the N-terminus, and residues 4−12 have been reported to be part of the α-helix (*45*). Penetratin and PenArg show essentially the same α-helical content in POPC/POPG vesicles, whereas PenLys has a somewhat more extended α-helix (Figures 3 and 4). Penetratin and PenArg also appear to have similar orientations of their Trp residues which can be seen in panels A and B of Figure 2. These residues are on average oriented with the plane of the indole chromophore parallel to the surface, giving a positive LD signal in the L_a and L_b region, but due to the spectral overlap of these transitions and the inherent difficulty in determining the orientation factor of the membrane, it was not considered meaningful in calculating more precise angles relative to the membrane surface.

The higher degree of α-helicity in PenLys (∼75% in POPC/POPG vesicles) means that both Trps can take part in the α-helix, thereby possibly changing the amphipathic face of the peptide and thus the orientation of the Trp residues. The Trp residues in PenLys do indeed have an orientation different from those of penetratin and PenArg, and the LD spectrum indicates that the L_b band is positive and the L_a band is negative. However, the LD signal in the L_a region becomes positive when cholesterol is present in the bilayer and the Trp residues in PenLys adopt an orientation more like that in penetratin and PenArg. This spectral change would be expected if the Trp residues are perpendicularly oriented to the membrane in a cholesterol-free environment and if introduction of cholesterol causes a tilt around the indole long axis, turning the Trps more parallel to the membrane. A possible explanation of this behavior is that cholesterol sterically prevents favorable hydrophobic interactions in the upper part of the hydrocarbon core, forcing the peptides to adopt a changed conformation in the more polar headgroup region in which an α-helical structure may be less rewarding. Such behavior has indeed been observed for amphipathic model peptide Ac-18A-NH_2 (*46*). It is also plausible that the change in conformation is due to the increased spacing of the headgroup region. Substituting the three C-terminal lysines in penetratin with arginines seems to be of little importance for the secondary structure when binding to pure POPC/POPG membranes, as evidenced from the similarities observed between penetratin and PenArg in LD and CD. By contrast, substitution of the two central arginines (residues 10 and 11) for lysines seems to have a profound effect both on the α-helicity and on the orientation of Trp in PenLys. It seems as if arginines are less likely to participate in adaptation of α-helical structure upon membrane binding than lysines. As can be seen in Figure 7, both residues 10 and 11 are on the more hydrophobic side of the penetratin peptides. Computer simulations have indicated that strong specific interactions between arginine residues and the phosphate groups of phospholipids exist (*47*), and the possibility of hydrogen bonding to lipid headgroups has been suggested to explain translocation of oligoarginines across bilayers (*17*). It is possible that favorable interactions that can be anticipated between the arginines at positions 10 and 11 in penetratin and, for example, lipid phosphate groups outweigh the gain in free energy from formation of a longer amphipathic helix.

As concluded above, all three penetratin peptides exhibit a high degree of orientation, and this is also in accordance with earlier reported results on penetratin (*44*). By contrast, TatP59W and R_7W have no LD signal in either the peptide bond region or the aromatic region of the spectra even though the binding isotherms in this study as well as previous studies clearly show that these peptides do bind to vesicle membranes (*15, 48*). It is worth comparing these two peptides to the very well oriented model compound TOE (*44*). TOE has an octyl carbon tail which can be inserted into the hydrocarbon core region serving to anchor this compound in the membrane, giving its indole chromophore less motional freedom. TatP59W and R_7W are rich in arginines and have a very flexible backbone structure because they are completely random coil. Even though it has been proposed that tryptophan has a strong preference for the membrane interface, close to the lipid carbonyls (*43*), it is more reasonable that the many charged residues have a stronger impact on membrane binding. A general observation is that TatP59W and R_7W, which are the most efficiently internalized CPPs in this study (see Table 1), do not adopt any preferred secondary structure upon membrane association. PenLys, on the contrary, is not internalized at all but has a high degree of secondary structure. Therefore, we suggest that backbone flexibility has an enhancing effect on internalization via direct membrane penetration. In addition, it has been shown that TatP59W and R_7W can cause fusion of LUVs which is not the case for penetratin (*48*). This is indeed an indication that these peptides have greater ability to perturb the membrane. Importantly, none of the three peptides have been observed to cause vesicle leakage (*11, 48*), and therefore, entry via pore formation can be ruled out. Nonendocytotic CPP entry has been suggested to occur by a mechanism where arginine residues form hydrogen bonds to negatively charged groups at the membrane surface, leading to a charge-neutralized complex that can penetrate the membrane (*17*). It has been suggested that backbone spacing is an important parameter for membrane transport of oligoarginines (*49*). One could speculate that the backbone spacing is needed to attain full charge neutralization by the rather bulky lipid headgroups and that this may be more efficient in TatP59W and R_7W since their random coil unordered structure allows them to adopt the most favorable orientation.

Experiments on depth-dependent tryptophan quenching by brominated lipids were performed to obtain an indication of Trp insertion depths and, accordingly, the peptide position. The insertion depths determined by the parallax equation are comparable to previously published data using vesicles with 40% surface charge (*14, 15*) in which the distance from the bilayer center was estimated to be 10−11 Å for all peptides. The estimated insertion depths suggest that the tryptophan residues are located in the hydrocarbon core region of the membrane which extends approximately 15 Å from the bilayer center in a DOPC membrane (*50*). Considering that the long-axis end-to-end distance in the indole chromophore is approximately 4 Å, it is possible for a peptide to reside in the headgroup region and still insert its tryptophan residues to this level. Still, the LD experiments show that the tryptophan residues in the penetratin peptides are more parallel than perpendicular to the membrane, and emission maximum wavelengths rather suggest interfacial positions

of the tryptophans which indicates that the insertion depths could be somewhat overestimated. However, since the estimated distance from the bilayer center (see Table 3) shows a slight tendency to increase with an increase in cholesterol concentration, discussing a possible effect of cholesterol on the degree of insertion is justified. Cholesterol, being inflexible in its structure and thus imposing rigidity on the upper part of the hydrocarbon core region, might provide resistance to the peptide in penetrating into the polar head region of the membrane. This result may suggest that tryptophan is penetrating into the hydrocarbon core in cholesterol-free membranes but that introduction of cholesterol pushes tryptophan and peptide into the membrane headgroup region. A similar effect of cholesterol has indeed been reported for the amphipathic Ac-18A-NH_2 peptide (*41*), and such an effect is also in agreement with the fact that the α-helical content is reduced with an increased cholesterol concentration as discussed above. By contrast, as will be further discussed below, fluorescence lifetime data from this study do not support this concept of changed penetration but are more in agreement with an unchanged environment around the tryptophan residues. Thus, the fact that the apparent insertion depth seems to vary with incorporation of cholesterol may be less significant, and we speculate that this effect may rather be a consequence of the membrane dynamics being affected in the presence of cholesterol. Altered lipid motion will affect the average proximity between the bromine quenchers and the tryptophan, and this dynamics is not considered in the current methods of analyzing depth-dependent quenching. However, to reach a true understanding of this behavior, more detailed studies would be necessary.

The quantum yields of Trp residues in the investigated peptides are comparable in magnitude (around 0.11) which is lower than that of free tryptophan (*35*). Moreover, these peptides adopt random coil structures in solution and exhibit very similar fluorescence emission maximum wavelengths. Taken together, these results indicate that the steady state emission properties of tryptophan in free peptides are affected little by the surrounding peptide residues. The slightly lower fluorescence quantum yield could be due to quenching by the carbonyl in the peptide bond (*33*) which can be brought closer to the Trp chromophore in a peptide. Association of peptide with membranes is generally accompanied by blue-shifted emission and an overall increase in fluorescence intensity. The fractional intensity increase upon membrane binding for the peptides in this study is dependent on cholesterol content (Figure 4). The penetratin peptides all exhibit significant decreases in intensity with an increased cholesterol concentration. This could be interpreted as tryptophan residues to some extent being more accessible to water in the latter case, which may be related to the structural change in terms of reduced α-helicity when cholesterol is incorporated into the membrane.

There is a significant variation in quantum yield for the different penetratin peptides associated with LUVs. The lysine-enriched penetratin analogue PenLys has the lowest quantum yield and the arginine-rich analogue PenArg the highest (Figure 4). This behavior correlates with the ability of these three peptides to enter live cells (see Table 1). Furthermore, in the same study, the R_7W peptide was proven to enter cells under two conditions that abolish endocytosis (low incubation temperature and depletion of intracellular ATP level), suggesting that a nonendocytotic pathway can lead to substantial peptide uptake. Even though R_7W displays weaker membrane binding than the penetratin peptides (see Figure 1), it shows the by far highest quantum yield in all types of LUVs used in this study. Also, TatP59W (which is an efficient CPP) has higher quantum yield than does penetratin, especially in LUVs containing cholesterol. It is tempting to attribute a higher quantum yield to deeper penetration and thereby more efficient shielding from water. However, this is not likely the explanation since both fluorescence emission maxima (Table 2) and lifetimes (Figure 6) indicate a peptide position within the headgroup region of the membrane. Moreover, the depth-dependent fluorescence quenching studies do not support such a systematic variation in insertion between different peptides. The variations in quantum yield are in fact more likely to result from different degrees of shielding from other quenchers of tryptophan fluorescence than water. Such quenchers may, for example, be lipid carbonyls in the headgroup region of the membrane. We suggest that the observed differences in quantum yields between the peptides in this study may reflect the fact that they have diverging abilities to cause local lipid rearrangement upon membrane binding and thus position the tryptophans in slightly different environments. As mentioned above, both R_7W and TatP59W cause vesicle fusion and are more prone to causing aggregation of liposomes than penetratin (*48*) and can hence more likely disturb the membrane which in turn may relate to how these peptides manage to enter cells via direct membrane penetration.

Several results in this study indicate that the tryptophan residues and, hence, the peptides reside in the headgroup region. The fluorescence emission maximum of the indole chromophore of tryptophan is sensitive to solvent polarity. The blue shift of approximately 12 nm from ~349 nm to slightly below 340 nm would be consistent with a permittivity (ϵ) of ~7 which is obviously lower than the polarity of the surrounding water but yet higher than the value in the hydrocarbon core region of the bilayer ($\epsilon \sim 2$) (*51*). Interestingly, the magnitude of the blue shift is not affected by an increase in the cholesterol content in the LUVs. The most obvious conclusion from this observation is that the tryptophan residues, and hence the peptides, do not reside in the hydrocarbon core region. This is further supported by the fact that the fluorescence lifetimes are largely invariant whether cholesterol is present. Since the tryptophan emission maximum is a rather rough estimate of insertion depth, detecting subtle changes in binding from such measurements is not conceivable.

The tryptophan fluorescence decay curves could be fitted satisfactorily using three exponentials (Figure 6), for both free and membrane-bound peptide. The existence of three lifetimes for a single tryptophan incorporated into a peptide has been reported before and could be explained by a rotamer model (*52*, *53*). This model postulates the existence of three distinguishable ground state conformers formed by rotation around the $C_\alpha - C_\beta$ bond axis. It has been suggested that conversion between two of these conformers is rapid and that only one lifetime can be detected from these two states (*53*) or that two conformers have very similar lifetimes in free tryptophan and are therefore not possible to distinguish

(*54*). Insertion into a peptide is likely to introduce additional constraints on the motional freedom around the $C_\alpha-C_\beta$ bond axis which hinder conversion on the time scale of fluorescence decay. The general trend is that lifetimes are increased when the peptide is bound to LUVs. This is in agreement with the observation of increased quantum yield. Incorporation of cholesterol into the vesicle membrane has no obvious systematic effect on the fluorescence lifetimes, and direct cholesterol−tryptophan interactions can thus be excluded. However, importantly, the lifetime measurements in the presence of cholesterol indicate that it is unlikely that the CPPs in this study should reside in the upper part of the hydrocarbon core region, since the properties of this part of the membrane are strongly affected by cholesterol incorporation which increases lipid chain order and reduces permeability. Thus, the fluorescence lifetime data support the notion that these CPPs reside mainly in the headgroup region of the membrane.

Apart from the fluorescence quantum yields, all tryptophan emission measurements point toward very small variations in membrane binding properties of the penetratin analogues, TatP59W and R_7W. These similarities could suggest that the variations that these peptides display in cells are not to be found in peptide−lipid interactions, and recent studies have in fact proposed that interactions with heparan sulfates are important for uptake of the full-length Tat protein (*55*, *56*) as well as for oligoarginines (*57*). However, the marked variations that we have observed in CD, LD, and fluorescence quantum yields emphasize that lipid interactions cannot be ruled out when possible uptake mechanisms of CPPs are being discussed.

In conclusion, our study on five cationic cell-penetrating peptides reveals a negative correlation between α-helicity and efficient internalization and shows a positive correlation between a large increase in fluorescence quantum yield upon membrane binding and CPP entry via direct membrane penetration. From our binding data, it is evident that arginine residues have a superior effect on binding affinity compared to lysines, but additionally, the central arginine residues in the penetratins seem to act as structural breakers that significantly reduce the α-helical content in penetratin and PenArg compared to that in nontranslocating PenLys. While penetratin enters cells only via endocytosis, PenArg, R_7W, and TatP59W do translocate into cells when endocytosis is shut down. In contrast to the penetratin peptides which do bind to membranes with a high degree of orientation, R_7W and TatP59W lack both secondary structure and an oriented binding mode. We discuss the importance of arginine residues in terms of charge neutralization by the formation of hydrogen bonds to negatively charged membrane components, but also the possible implications of backbone flexibility for efficient entry via direct membrane penetration, and hypothesize that backbone flexibility may be necessary to attain sufficient charge neutralization so that the CPP can be dissolved in the bilayer interior and thereby enter the cell. We also note that the large increase in the quantum yield for R_7W and TatP59W may be connected to their ability to cause vesicle fusion and aggregation and that such lipid rearrangement may relate to efficient membrane translocation.

ACKNOWLEDGMENT

We thank Mikael Winters for his help with the SPC measurements and Prof. Bo Albinsson for interpretation and analysis of SPC data.

REFERENCES

1. Frankel, A. D., and Pabo, C. O. (1988) Cellular uptake of the tat protein from human immunodeficiency virus, *Cell 55*, 1189−93.
2. Green, M., and Loewenstein, P. M. (1988) Autonomous functional domains of chemically synthesized human immunodeficiency virus tat trans-activator protein, *Cell 55*, 1179−88.
3. Vives, E., Brodin, P., and Lebleu, B. (1997) A truncated HIV-1 Tat protein basic domain rapidly translocates through the plasma membrane and accumulates in the cell nucleus, *J. Biol. Chem. 272*, 16010−7.
4. Wender, P. A., Mitchell, D. J., Pattabiraman, K., Pelkey, E. T., Steinman, L., and Rothbard, J. B. (2000) The design, synthesis, and evaluation of molecules that enable or enhance cellular uptake: Peptoid molecular transporters, *Proc. Natl. Acad. Sci. U.S.A. 97*, 13003−8.
5. Derossi, D., Calvet, S., Trembleau, A., Brunissen, A., Chassaing, G., and Prochiantz, A. (1996) Cell internalization of the third helix of the Antennapedia homeodomain is receptor-independent, *J. Biol. Chem. 271*, 18188−93.
6. Vives, E., Granier, C., Prevot, P., and Lebleu, B. (1997) Structure−activity relationship study of the plasma membrane translocating potential of a short peptide from HIV-1 Tat protein, *Lett. Pept. Sci. 4*, 429−36.
7. Joliot, A., Pernelle, C., Deagostini-Bazin, H., and Prochiantz, A. (1991) Antennapedia homeobox peptide regulates neural morphogenesis, *Proc. Natl. Acad. Sci. U.S.A. 88*, 1864−8.
8. Drin, G., Demene, H., Temsamani, J., and Brasseur, R. (2001) Translocation of the pAntp peptide and its amphipathic analogue AP-2AL, *Biochemistry 40*, 1824−34.
9. Magzoub, M., Eriksson, L. E., and Graslund, A. (2003) Comparison of the interaction, positioning, structure induction and membrane perturbation of cell-penetrating peptides and non-translocating variants with phospholipid vesicles, *Biophys. Chem. 103*, 271−88.
10. Persson, D., Thoren, P. E., and Norden, B. (2001) Penetratin-induced aggregation and subsequent dissociation of negatively charged phospholipid vesicles, *FEBS Lett. 505*, 307−12.
11. Thoren, P. E., Persson, D., Karlsson, M., and Norden, B. (2000) The antennapedia peptide penetratin translocates across lipid bilayers: The first direct observation, *FEBS Lett. 482*, 265−8.
12. Lundberg, M., and Johansson, M. (2002) Positively charged DNA-binding proteins cause apparent cell membrane translocation, *Biochem. Biophys. Res. Commun. 291*, 367−71.
13. Richard, J. P., Melikov, K., Vives, E., Ramos, C., Verbeure, B., Gait, M. J., Chernomordik, L. V., and Lebleu, B. (2003) Cell-penetrating peptides. A reevaluation of the mechanism of cellular uptake, *J. Biol. Chem. 278*, 585−90.
14. Persson, D., Thoren, P. E., Esbjorner, E. K., Goksor, M., Lincoln, P., and Norden, B. (2004) Vesicle size-dependent translocation of penetratin analogs across lipid membranes, *Biochim. Biophys. Acta 1665*, 142−55.
15. Thoren, P. E., Persson, D., Esbjorner, E. K., Goksor, M., Lincoln, P., and Norden, B. (2004) Membrane binding and translocation of cell-penetrating peptides, *Biochemistry 43*, 3471−89.
16. Terrone, D., Sang, S. L., Roudaia, L., and Silvius, J. R. (2003) Penetratin and related cell-penetrating cationic peptides can translocate across lipid bilayers in the presence of a transbilayer potential, *Biochemistry 42*, 13787−99.
17. Rothbard, J. B., Jessop, T. C., Lewis, R. S., Murray, B. A., and Wender, P. A. (2004) Role of membrane potential and hydrogen bonding in the mechanism of translocation of guanidinium-rich peptides into cells, *J. Am. Chem. Soc. 126*, 9506−7.
18. Thoren, P. E., Persson, D., Isakson, P., Goksor, M., Onfelt, A., and Norden, B. (2003) Uptake of analogs of penetratin, Tat(48−60) and oligoarginine in live cells, *Biochem. Biophys. Res. Commun. 307*, 100−7.
19. Fittipaldi, A., Ferrari, A., Zoppe, M., Arcangeli, C., Pellegrini, V., Beltram, F., and Giacca, M. (2003) Cell membrane lipid rafts mediate caveolar endocytosis of HIV-1 Tat fusion proteins, *J. Biol. Chem. 278*, 34141−9.

20. Wadia, J. S., Stan, R. V., and Dowdy, S. F. (2004) Transducible TAT-HA fusogenic peptide enhances escape of TAT-fusion proteins after lipid raft macropinocytosis, *Nat. Med. 10*, 310−5.
21. Nakase, I., Niwa, M., Takeuchi, T., Sonomura, K., Kawabata, N., Koike, Y., Takehashi, M., Tanaka, S., Ueda, K., Simpson, J. C., Jones, A. T., Sugiura, Y., and Futaki, S. (2004) Cellular uptake of arginine-rich peptides: Roles for macropinocytosis and actin rearrangement, *Mol. Ther. 10*, 1011−22.
22. Saalik, P., Elmquist, A., Hansen, M., Padari, K., Saar, K., Viht, K., Langel, U., and Pooga, M. (2004) Protein cargo delivery properties of cell-penetrating peptides. A comparative study, *Bioconjugate Chem. 15*, 1246−53.
23. Persson, D., Thoren, P. E. G., Lincoln, P., and Norden, B. (2004) Vesicle membrane interactions of penetratin analogues, *Biochemistry 43*, 11045−55.
24. Lipowsky, R., and Sackmann, E. (1995) *Structure and dynamics of membranes*, Elsevier, Amsterdam.
25. Subczynski, W. K., Wisniewska, A., Yin, J. J., Hyde, J. S., and Kusumi, A. (1994) Hydrophobic barriers of lipid bilayer membranes formed by reduction of water penetration by alkyl chain unsaturation and cholesterol, *Biochemistry 33*, 7670−81.
26. Levine, Y. K. (1972) Physical studies of membrane structure, *Prog. Biophys. Mol. Biol. 24*, 1−74.
27. Yeagle, P. L., Hutton, W. C., Huang, C., and Martin, R. B. (1977) Phospholipid head-group conformations; intermolecular interactions and cholesterol effects, *Biochemistry 16*, 4344−9.
28. Ohvo-Rekila, H., Ramstedt, B., Leppimaki, P., and Slotte, J. P. (2002) Cholesterol interactions with phospholipids in membranes, *Prog. Lipid Res. 41*, 66−97.
29. Jedlovszky, P., and Mezei, M. (2003) Effect of cholesterol on the properties of phospholipid membranes. 1. Structural features, *J. Phys. Chem. B 107*, 5311−21.
30. Ardhammar, M., Lincoln, P., and Norden, B. (2002) Invisible liposomes: Refractive index matching with sucrose enables flow dichroism assessment of peptide orientation in lipid vesicle membrane, *Proc. Natl. Acad. Sci. U.S.A. 99*, 15313−7.
31. Ardhammar, M., Mikati, N., and Norden, B. (1998) Chromophore orientation in liposome membranes probed with flow dichroism, *J. Am. Chem. Soc. 120*, 9957−9958.
32. Norden, B., Kubista, M., and Kurucsev, T. (1992) Linear Dichroism Spectroscopy of Nucleic-Acids, *Q. Rev. Biophys. 25*, 51−170.
33. Chen, Y. H., Yang, J. T., and Chau, K. H. (1974) Determination of Helix and β-Form of Proteins in Aqueous Solution by Circular Dichroism, *Biochemistry 13*, 3350−3359.
34. Persson, D., Thoren, P. E., Herner, M., Lincoln, P., and Norden, B. (2003) Application of a novel analysis to measure the binding of the membrane-translocating peptide penetratin to negatively charged liposomes, *Biochemistry 42*, 421−9.
35. Lakowicz, J. R. (1999) *Principles of Fluorescence Spectroscopy*, 2nd ed., Kluwer Academic/Plenum Publishers, New York.
36. Chattopadhyay, A., and London, E. (1987) Parallax method for direct measurement of membrane penetration depth utilizing fluorescence quenching by spin-labeled phospholipids, *Biochemistry 26*, 39−45.
37. McIntosh, T. J., and Holloway, P. W. (1987) Determination of the depth of bromine atoms in bilayers formed from bromolipid probes, *Biochemistry 26*, 1783−8.
38. Lewis, B. A., and Engelman, D. M. (1983) Lipid bilayer thickness varies linearly with acyl chain length in fluid phosphatidylcholine vesicles, *J. Mol. Biol. 166*, 211−7.
39. Lundberg, B. (1982) A Surface-Film Study of the Lateral Packing of Phosphatidyl-Choline and Cholesterol, *Chem. Phys. Lipids 31*, 23−32.
40. Beschiaschvili, G., and Seelig, J. (1990) Peptide binding to lipid bilayers. Binding isotherms and zeta-potential of a cyclic somatostatin analogue, *Biochemistry 29*, 10995−1000.
41. Egashira, M., Gorbenko, G., Tanaka, M., Saito, H., Molotkovsky, J., Nakano, M., and Handa, T. (2002) Cholesterol modulates interaction between an amphipathic class A peptide, Ac-18A-NH_2, and phosphatidylcholine bilayers, *Biochemistry 41*, 4165−72.
42. Nagle, J. F., Zhang, R. T., TristramNagle, S., Sun, W. J., Petrache, H. I., and Suter, R. M. (1996) X-ray structure determination of fully hydrated L(α) phase dipalmitoylphosphatidylcholine bilayers, *Biophys. J. 70*, 1419−31.
43. Yau, W. M., Wimley, W. C., Gawrisch, K., and White, S. H. (1998) The preference of tryptophan for membrane interfaces, *Biochemistry 37*, 14713−8.
44. Brattwall, C. E., Lincoln, P., and Norden, B. (2003) Orientation and conformation of cell-penetrating peptide penetratin in phospholipid vesicle membranes determined by polarized-light spectroscopy, *J. Am. Chem. Soc. 125*, 14214−5.
45. Czajlik, A., Mesko, E., Penke, B., and Perczel, A. (2002) Investigation of penetratin peptides. Part 1. The environment dependent conformational properties of penetratin and two of its derivatives, *J. Pept. Sci. 8*, 151−71.
46. Gorbenko, G., Handa, T., Saito, H., Molotkovsky, J., Tanaka, M., Egashira, M., and Nakano, M. (2003) Effect of cholesterol on bilayer location of the class A peptide Ac-18A-NH_2 as revealed by fluorescence resonance energy transfer, *Eur. Biophys. J. 32*, 703−9.
47. Ulmschneider, M. B., and Sansom, M. S. (2001) Amino acid distributions in integral membrane protein structures, *Biochim. Biophys. Acta 1512*, 1−14.
48. Thoren, P. E. G., Persson, D., Lincoln, P., and Norden, B. (2005) Membrane destabilizing properties of cell-penetrating peptides, *Biophys. Chem. 114*, 169−79.
49. Rothbard, J. B., Kreider, E., VanDeusen, C. L., Wright, L., Wylie, B. L., and Wender, P. A. (2002) Arginine-rich molecular transporters for drug delivery: Role of backbone spacing in cellular uptake, *J. Med. Chem. 45*, 3612−8.
50. Wiener, M. C., and White, S. H. (1992) Structure of a Fluid Dioleoylphosphatidylcholine Bilayer Determined by Joint Refinement of X-ray and Neutron-Diffraction Data. 3. Complete Structure, *Biophys. J. 61*, 434−47.
51. Beschiaschvili, G., and Seelig, J. (1991) Peptide binding to lipid membranes. Spectroscopic studies on the insertion of a cyclic somatostatin analog into phospholipid bilayers, *Biochim. Biophys. Acta 1061*, 78−84.
52. Fleming, G. R., Morris, J. M., Robbins, R. J., Woolfe, G. J., Thistlethwaite, P. J., and Robinson, G. W. (1978) Non-Exponential Fluorescence Decay of Aqueous Tryptophan and 2 Related Peptides by Picosecond Spectroscopy, *Proc. Natl. Acad. Sci. U.S.A. 75*, 4652−6.
53. Szabo, A. G., and Rayner, D. M. (1980) Fluorescence Decay of Tryptophan Conformers in Aqueous-Solution, *J. Am. Chem. Soc. 102*, 554−63.
54. Petrich, J. W., Chang, M. C., McDonald, D. B., and Fleming, G. R. (1983) On the Origin of Non-Exponential Fluorescence Decay in Tryptophan and Its Derivatives, *J. Am. Chem. Soc. 105*, 3824−32.
55. Rusnati, M., Tulipano, G., Spillmann, D., Tanghetti, E., Oreste, P., Zoppetti, G., Giacca, M., and Presta, M. (1999) Multiple interactions of HIV-I Tat protein with size-defined heparin oligosaccharides, *J. Biol. Chem. 274*, 28198−205.
56. Tyagi, M., Rusnati, M., Presta, M., and Giacca, M. (2001) Internalization of HIV-1 tat requires cell surface heparan sulfate proteoglycans, *J. Biol. Chem. 276*, 3254−61.
57. Fuchs, S. M., and Raines, R. T. (2004) Pathway for polyarginine entry into mammalian cells, *Biochemistry 43*, 2438−44.

BI052095T